JCB Article

Oligodendroglial modulation of fast axonal transport in a mouse model of hereditary spastic paraplegia

Julia M. Edgar,[1] Mark McLaughlin,[1] Donald Yool,[1] Su-Chun Zhang,[3] Jill H. Fowler,[2] Paul Montague,[1] Jennifer A. Barrie,[1] Mailis C. McCulloch,[1] Ian D. Duncan,[3] James Garbern,[4] Klaus A. Nave,[5] and Ian R. Griffiths[1]

[1]Applied Neurobiology Group, Institute of Comparative Medicine, and [2]Clinical Neuroscience, Wellcome Surgical Institute, University of Glasgow, Glasgow G61 1QH, Scotland, UK
[3]Department of Medical Sciences, School of Veterinary Medicine, University of Wisconsin-Madison, Madison, WI 53706
[4]Department of Neurology and Center for Molecular Medicine and Genetics, Wayne State University, Detroit, MI 48201
[5]Department of Neurogenetics, Max Planck Institute of Experimental Medicine, D-37075 Goettingen, Germany

Oligodendrocytes are critical for the development of the plasma membrane and cytoskeleton of the axon. In this paper, we show that fast axonal transport is also dependent on the oligodendrocyte. Using a mouse model of hereditary spastic paraplegia type 2 due to a null mutation of the myelin *Plp* gene, we find a progressive impairment in fast retrograde and anterograde transport. Increased levels of retrograde motor protein subunits are associated with accumulation of membranous organelles distal to nodal complexes. Using cell transplantation, we show categorically that the axonal phenotype is related to the presence of the overlying *Plp* null myelin. Our data demonstrate a novel role for oligodendrocytes in the local regulation of axonal function and have implications for the axonal loss associated with secondary progressive multiple sclerosis.

Introduction

The hereditary spastic paraplegias (HSPs) are a diverse group of clinical syndromes in which the spastic paraparesis/paraplegia may be the sole or predominant sign (pure forms) or may coexist with other neurological deficits (complicated forms). The essential pathology of HSP is degeneration of the distal regions of the corticospinal tracts with preservation of their cell bodies. The disorders map to at least 18 loci and may be inherited as autosomal-dominant or -recessive or X-linked traits (for reviews see Crosby and Proukakis, 2002; Fink, 2002; Reid, 2003). In the minority of loci where a causal gene has been identified there is no obvious commonality, with the products showing structural and functional diversity often targeted to different locations in the cell and expressed in various cell types. Many of the candidate genes are expressed ubiquitously and show no preferential expression for the subset(s) of neurons affected in HSP. The pathogenesis of these disorders remains obscure, although a failure in axonal transport has been proposed as a common mechanism (Crosby and Proukakis, 2002) and *KIF5A*, encoding a neuronal-specific kinesin, has been identified as the causal gene for spastic paraplegia type 10 (Reid et al., 2002).

X-linked spastic paraplegia type 2 is caused by mutations of the proteolipid protein 1 (*PLP1*) gene, which encodes PLP and its minor DM20 isoform, the major proteins of the myelin sheath. One intriguing question is why mutations of a gene expressed in oligodendrocytes leads to degeneration of axons. Complete absence of PLP/DM20 due to gene deletion or null mutation is associated with spastic paraplegia type 2 and mild forms of Pelizaeus-Merzbacher disease. In *Plp* null mice, the majority of axons are surrounded by an appropriate thickness of myelin, which shows variable defects of the intraperiod line but otherwise remains intact throughout life (Klugmann et al., 1997). Axonal swellings (spheroids) resulting from accumulations of membranous organelles arise in small-diameter axons; such spheroids are often associated with paranodal areas (Griffiths et al., 1998). Older

The online version of this article includes supplemental material.

Address correspondence to I.R. Griffiths, Applied Neurobiology Group, Dept. of Veterinary Clinical Studies, University of Glasgow, Bearsden, Glasgow G61 1QH, Scotland, UK. Tel.: 0141-330-5806. Fax: 0141-942-7215. email: I.Griffiths@vet.gla.ac.uk

D. Yool's present address is Dept. of Veterinary Clinical Studies, Royal (Dick) School of Veterinary Studies, Hospital for Small Animals, Easter Bush Veterinary Centre, Roslin EH25 9RG, Scotland, UK.

Key words: proteolipid protein; oligodendrocyte; axonal transport; hereditary spastic paraplegia; axonal degeneration

Abbreviations used in this paper: CTB, cholera toxin B subunit; HSP, hereditary spastic paraplegia; MBP, myelin basic protein; NF, neurofilament; PLP, proteolipid protein; RGC, retinal ganglion cell.

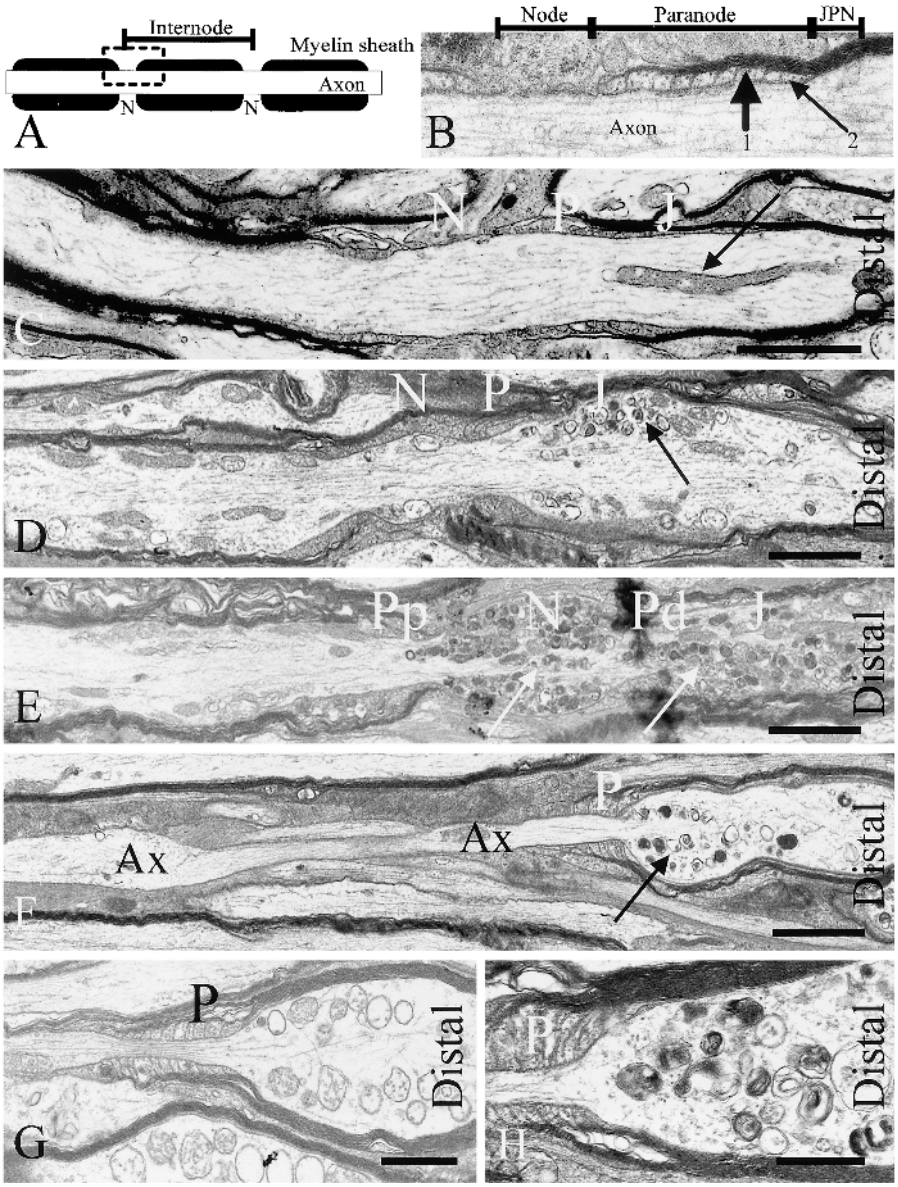

Figure 1. **Membranous organelles accumulate preferentially distal to the nodal complex in optic nerve axons of PLP/DM20-deficient mice.** (A) Schematic showing the axon and surrounding myelin sheath. The length of axon myelinated by a single oligodendrocyte process is termed the internode and terminates at the nodes of Ranvier (N). (B) The boxed area from A is shown in detail. The node of Ranvier is abutted by the paranode, the region at which the terminal loops of individual myelin lamellae (arrow 1) appose the axolemma in an orderly manner. The juxtaparanode (JPN) is the region between the paranode and the internode. The paranodal axo–glial junction (arrow 2) is a highly specialized intercellular junction (shown in more detail in Fig. S1 D, available at http://www.jcb.org/cgi/content/full/jcb.200312012/DC1). (C) Wild-type axon showing a nodal complex. The node (N), paranode (P), and juxtaparanodal (J) regions are indicated, as is the distal (chiasmal) side. In this particular example only one axonal mitochondrion is evident (arrow), although in other instances several organelles may be present. Bar, 2 μm. (D) In this and subsequent images the axons are from *Plp* null mice. A small accumulation of dense bodies and mitochondria (arrow) are present at the distal juxtaparanode (J). The proximal juxtaparanode and internode contain several nonclustered mitochondria, which is slightly in excess of the maximum number observed in wild-type axons. However, there is a distinct difference between proximal and distal regions. Bar, 2 μm. (E) In this example the accumulated dense bodies and mitochondria occupy the distal internode, juxtaparanode (J), and paranode (Pd), and have also extended into the nodal (N) region; the proximal paranode (Pp) remains unaffected. Bar, 2 μm. (F) A proportion of optic nerve axons in *Plp* null mice have nonmyelinated regions interposed between myelinated internodes. In this example the proximal axon (Ax) is unmyelinated, whereas the distal axon is myelinated. A heminode with its paranode (P) is present. A collection of organelles, predominantly dense bodies (arrow), is present distal to the paranode, whereas no accumulation is present proximally. Bar, 2 μm. (G) The distal aspect of a nodal complex is shown with the paranode (P) marked. The distal axon contains a small accumulation of mitochondria. Bar, 1 μm. (H) Another axon shows accumulation of dense bodies distal to the paranode (P). Bar, 1 μm.

mice develop an age- and length-dependent degeneration of long spinal tracts, such as the fasciculus gracilis (Garbern et al., 2002). Human patients lacking PLP/DM20 due to a null mutation also show extensive axonal degeneration in the distal corticospinal tracts and fasciculus gracilis and a more diffuse axonal loss throughout much of the cerebral white matter; surviving axons are surrounded by myelin sheaths (Garbern et al., 2002). Therefore, absence of the myelin protein PLP/DM20 results in diffuse axonal swellings and selective axonal degeneration of specific long spinal tracts in both man and mouse.

In this paper, we test and verify the hypothesis that absence of PLP/DM20 in oligodendrocytes impairs fast axonal transport. This provides the first direct functional demonstration of a pathogenetic mechanism for any of the HSP disorders, and offers a further insight into how oligodendrocytes influence the function of axons.

Results

Membranous organelles accumulate preferentially at the distal juxtaparanode

To ascertain the evolution of axonal changes, we examined the optic nerves of *Plp* null mice at P20, 40, 60, and 120. No definitive changes were recognized at P20, but by P40 focal accumulations of membranous organelles, principally dense bodies and mitochondria, were present. These increased in frequency and extent by P120. Consistent with

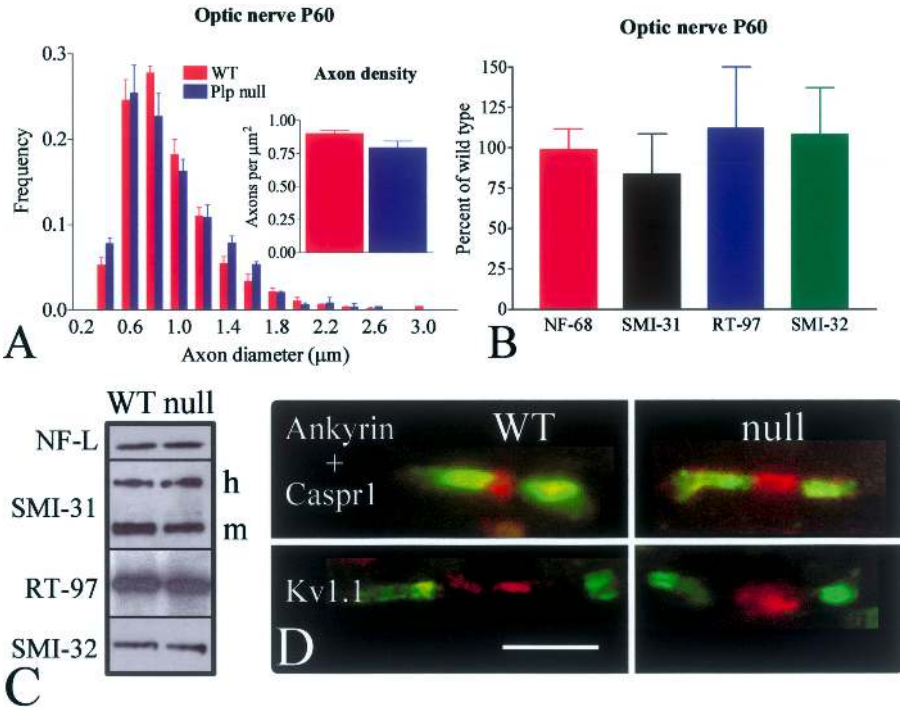

Figure 2. **Absence of PLP/DM20 in oligodendrocytes does not impair the differentiation of axonal cytoskeleton and axolemma.** (A) Axonal diameter frequency distributions from optic nerves of P60 wild-type and *Plp* null mice; the profiles are identical. (M ± SEM; $n = 4$). Inset: axonal densities in the optic nerve are also unaltered in the *Plp* null mice at P60. (M ± SEM; $n = 4$). (B) Levels of NF proteins in the triton-insoluble fraction from optic nerves of P60 *Plp* null mice are not different from wild-type littermates. (M ± SEM; $n = 4$ or 5). Similar results were found using the cytoskeletal-enriched fraction from brain and spinal cord (C). Representative immunoblots: NF-L recognizes the light chain NF, SMI-31 recognizes phosphorylated epitopes on the NF-H (h) and NF-M (m) polypeptides; RT-97 recognizes a different phosphorylated epitope on NF-H, and SMI-32 detects nonphosphorylated epitopes on NF-H. (D) Molecular markers for the node, ankyrin (red) and axolemma of the paranode, caspr-1 (green), and juxtaparanode, Kv1.1 (green) in P60 optic nerves from wild-type (WT) and *Plp* null (KO) mice. The localization appears similar in both genotypes. The Kv1.1 staining of the juxtaparanode is separated from the node by a gap, which represents the paranodal region. Bar, 5 μm.

our earlier report (Griffiths et al., 1998), we noted a tendency for organelles to accumulate distal to a nodal complex, often commencing in the region of the juxtaparanode (see Fig. 1, A and B for terminology) and then extending. The axon proximal to the node was either normal or was affected to a much lesser degree (Fig. 1, D–F). Quantification at P40 showed that the frequency of accumulations was much greater on the distal (51.3 ± 4.9%) compared with the proximal (12.1 ± 5%; P = 0.001) side of the node. Changes in the null mice were also significantly different from the wild type, in which organelle accumulation was noted at 3.7 ± 1% of distal and 0% of proximal nodal regions. At P40 the *Plp* null axons were seldom swollen, but by P60 and subsequently focal swellings and associated attenuation of the overlying sheath were evident in some fibers (Fig. S1, A–C; available at http://www.jcb.org/cgi/content/full/jcb.200312012/DC1). The swellings were present along the length of the optic nerve, the tract, and in the brachium of the superior colliculus (unpublished data). The axonal cytoskeletal organization was disrupted within and immediately adjacent to the area of the accumulations/swellings. Neurofilaments (NFs) and microtubules were either displaced to a small domain of the axon or replaced by a fine granular amorphous material (Fig. 1, G and H). Outside of the focal accumulations of organelles, the organization of the axonal cytoskeleton appeared normal. The paranodal axo–glial junction was intact with regular arrays of transverse bands on the external axolemma (Fig. S1 D). Occasional myelinated fibers undergoing Wallerian degeneration were noted in the optic nerve at P120.

Accumulation of axonal organelles relates to PLP-deficient myelin

Due to random X-inactivation, $Plp^{+/-}$ heterozygotes are chimeras in which internodes may be formed from PLP/DM20+ or PLP/DM20-deficient myelin (Yool et al., 2001). Using the optic nerve, we determined whether the accumulations of membranous organelles were biased toward one population of internodes. At P40, all accumulations of organelles (n mice = 3; n spheroids examined = 67) were associated with PLP/DM20-deficient myelin, and even at one year of age 95 ± 3% (n mice = 3; n spheroids = 48) remained associated with such internodes. These findings suggest that once formed, the spheroids show little tendency to migrate along the axon.

Differentiation of the axonal cytoskeleton and axolemma occurs in the absence of PLP/DM20

Regional differentiation of the axolemma, phosphorylation of the axonal cytoskeleton, and ultimately axonal size (Brady et al., 1999; Gotow et al., 1999; Sánchez et al., 2000; Kirkpatrick et al., 2001) depend on contact with myelin-forming oligodendrocytes. Axonal diameter frequency distributions and axonal density in the optic nerve (Fig. 2 A) and ventral spinal cord of wild-type and *Plp* null mice at P20 and P60 were similar. No difference was detected in the NF populations of the optic nerve and spinal cord of *Plp* null mice at P20 and P60 by Western blotting (Fig. 2, B and C) or immunostaining (unpublished data). Caspr-1 and Kv1.1, molecular markers of the paranode and juxtaparanode, respectively (Peles and Salzer, 2000), were present in *Plp* null mice

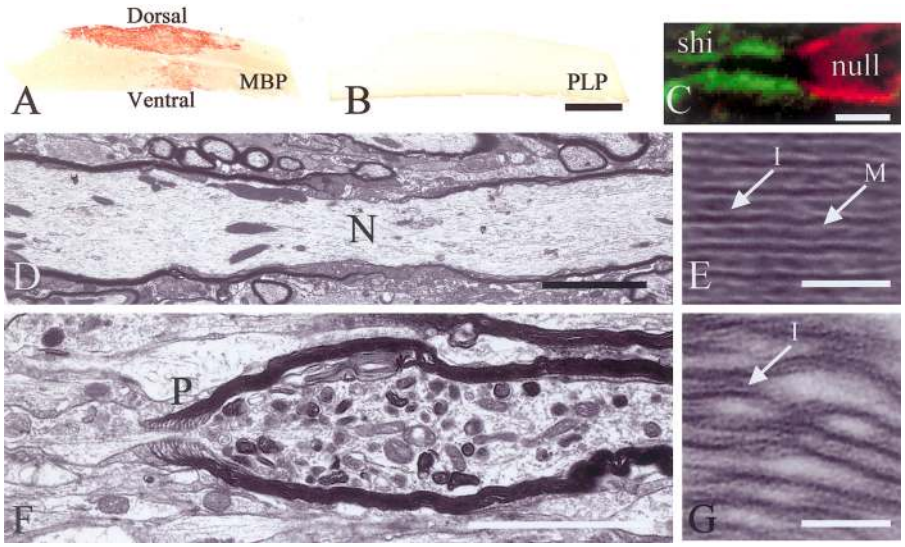

Figure 3. **PLP/DM20-deficient oligodendrocytes induce a focal axonopathy when transplanted into the dorsal columns of shiverer mice.** (A and B) Adjacent longitudinal resin sections of *shiverer* spinal cord transplanted with *Plp* null cells and immunostained for MBP (A) and PLP (B). The majority of myelin is in the dorsal columns. The transplanted myelin stains strongly for MBP (A), but is negative for PLP (B). Bar, 1 mm. When using this method of processing on resin sections, only the compact myelin of the transplant is immunostained. (C) *shiverer* axons are ensheathed, rather than myelinated, by oligodendrocyte processes that are PLP+/MBP−, and a cryosection immunostained for PLP (green) and MBP (red) shows two fibers at the junction between the host shiverer processes (shi) and the PLP−/MBP+ myelin produced by the transplanted *Plp* null cells (null). Bar, 20 μm. (D) Myelination by transplanted wild-type cells showing a node (N) and normal axonal appearance. Bar, 2 μm. (E) Part of the wild-type myelin sheath with major dense (M, arrow) and intraperiod (I, arrow) lines. Bar, 50 nm. (F) Myelination by transplanted *Plp* null cells showing an axon containing numerous membranous organelles adjacent to a paranode (P). Bar, 2 μm. (G) Part of the PLP-deficient myelin sheath showing widening of the intraperiod line. Bar, 50 nm.

(Fig. 2 D) as were the paranodal transverse bands (Fig. S1 D). Neurofascin, which marks the oligodendrocyte paranodal loops, was also present (unpublished data).

Absence of PLP/DM20 in the oligodendrocyte induces a local axonopathy

To demonstrate unequivocally that the axonopathy resulted only from absence of PLP/DM20 in the overlying oligodendrocyte, we transplanted neurospheres from *Plp* null or wild-type mice into the dorsal columns of the myelin-deficient *shiverer* mutant. The transplanted myelin basic protein (MBP+) myelin was clearly distinguishable against the negative background of the *shiverer* host (Fig. 3, A–C). None of the mice (0/7) myelinated by transplanted wild-type cells developed any axonal abnormalities (Fig. 3 D; Fig. S2 A, available at http://www.jcb.org/cgi/content/full/jcb.200312012/DC1), whereas all (4/4) of the grafts myelinated by *Plp* null cells contained axonal changes characterized by accumulation of membranous organelles, sometimes adjacent to paranodes (Fig. 3 F). The myelin sheaths generated by the *Plp* null cells (Fig. 3 G) showed the characteristic changes described previously (Boison et al., 1995; Yool et al., 2002a) in comparison with the wild-type myelin (Fig. 3 E). By EM, 1–3 abnormal axons were detected per grid square (9,409 μ^2) of the PLP-deficient transplants (Fig. S2, B–D). No alterations were noted in *shiverer* axons outside the grafted region.

Absence of PLP impairs fast axonal transport systems

The accumulation of axonal membranous organelles distal to the node in the optic nerves of PLP/DM20-deficient mice resembles the situation described distal to a cold block in the sciatic nerve (Tsukita and Ishikawa, 1980), suggesting defects in retrograde axonal transport. We examined this parameter more directly by injecting FITC-conjugated cholera toxin B (CTB) into the superior colliculus and measuring its accumulation in retinal ganglion cells (RGCs) 12 h after injection at 1, 2, 4, 12, and 18 mo of age (Fig. 4 A). Significantly less tracer was evident in the retina in *Plp* null mice from 2 mo onward, the deficit worsening with age (Fig. 4, B and C). The number of optic nerve axons (Fig. 2 A) and the size of the RGCs (Fig. 4 D) were not significantly different at P60, indicating these factors did not account for the reduction in the measured fluorescent signal. When a labeling time of 6 h was used in 4-mo-old mice, fewer, less intensely stained RGCs were detected in the null; the signal being 63% of wild type. No RGC labeling was seen in either genotype 3 h after injection. When the labeling interval was extended to 3 d the level of signal increased considerably in wild type, but remained the same as for 12 h in the null mice so that fluorescence was now only 31% of control. Focal accumulations of fluorescent tracer were found along the entire length of the optic nerve in the *Plp* null mice, but occurred only rarely in the wild type (Fig. 4, E–G).

We used a similar strategy to examine the accumulation of anterogradely transported proteins 12 h after intraocular injection of [^{35}S]methionine. At 2 mo, there was no difference in the accumulation of radiolabeled proteins in the superior colliculus of *Plp* null compared with the wild-type mice. By 4 mo, a 25% reduction was evident, which increased to 54% by 18 mo (Fig. 4 H). Immunostaining for βAPP is often used to demonstrate defects in axonal transport. Immunostaining of brain and optic nerve for βAPP and ubiquitin revealed small focal swellings in white matter from ∼2 mo of age (unpublished data). The frequency of the βAPP+ swellings did not appear to increase between 3 mo and 1 year.

Levels of retrograde motor and associated proteins are elevated in the absence of PLP

To further evaluate the defects in axonal transport, we quantified the levels of dynein intermediate chain and dynactin p50, together with the heavy chain subunits of kinesin, in triton-soluble extracts of optic nerves from *Plp* null mice and

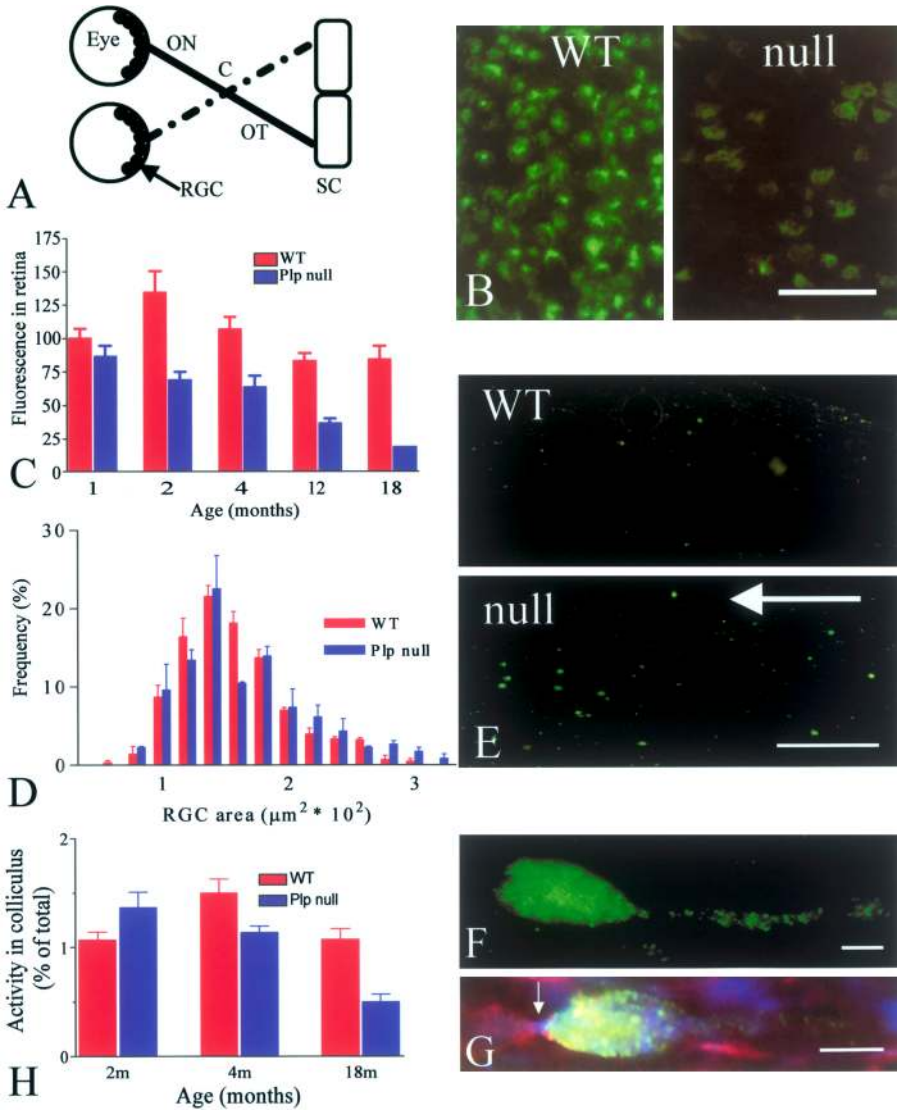

Figure 4. **Absence of PLP/DM20 is associated with impaired fast retrograde and anterograde axonal transport.** (A) Schematic of the optic pathways showing the eye, optic nerve (ON), chiasm (C), optic tract (OT), and superior colliculus (SC). The distal optic tract continues as the brachium of the superior colliculus (not depicted) to terminate in the optic nerve layer of the colliculus. In rodents, >90% of axons in the optic nerve decussate at the chiasm and terminate in the contralateral superior colliculus. The RGCs are the cell bodies of axons that terminate in the colliculus. (B) Area of retinal whole mount from wild-type (WT) and *Plp* null (null) littermates aged 4 mo, 12 h after injection of FITC-conjugated CTB into the superior colliculus; images were collected and processed identically. The number of labeled RGCs and the intensity of fluorescence are much greater in the wild type. Bar, 50 μm. (C) Accumulation of retrogradely transported CTB-FITC 12 h after injection into the superior colliculus in wild-type and *Plp* null littermates of denoted ages. The signal in the RGCs is expressed as fluorescence area ($\mu m^2/mm^2$) of retina. (M ± SEM; $n = 4$ or 5). The difference between the two genotypes is significant at all ages except 1 mo. (D) Frequency distribution of RGC body area as defined by immunostaining for β-tubulin III in wild-type and *Plp* null littermates at P60. (M ± SEM; $n = 2$). There is no difference between the two genotypes. (E) Longitudinal sections of optic nerves from wild-type (WT) and *Plp* null mice at 4 mo of age, 48 h after injection of FITC-conjugated CTB into the superior colliculus. Only an occasional focus of fluorescent labeling is observed in the wild type, whereas numerous CTB-filled axonal swellings are evident along the *Plp* null nerve. The direction of retrograde transport is indicated by the arrow. Bar, 200 μm. (F) Enlargement of single swelling from E, showing a "tail" of tracer in the axon distal to the swelling. Bar, 10 μm. (G) Section from the nerve shown in E, immunostained for caspr-1 (red) and NFs (blue). The FITC-conjugated CTB has accumulated distal to the nodal complex. The node (arrow) is bounded by the caspr-1–stained paranodes. The caspr-1 staining above and below the swelling belongs to other axons. Note the punctate staining of the CTB, suggesting its presence in membranous components such as endosomes. Bar, 5 μm. (H) Accumulation of fast anterogradely transported protein in the superior colliculi of wild-type and *Plp* null mice at ages 2, 4, and 18 mo. The radiolabeled protein in the colliculi is expressed as a percentage of the total TCA-precipitated labeled material in the optic system. (M ± SEM; $n = 5$–7). The differences at 4 and 18 mo are significant.

wild-type littermates at P20 (unpublished data) and P60 (Fig. 5, A and B). Using the preparative technique (see Materials and methods), this fraction will contain detergent-extracted membrane proteins. The selected ages represent times just before and after definitive ultrastructural evidence of an axonopathy, respectively. Levels of dynein and dynactin were significantly increased at both ages, more markedly at P60, whereas kinesin levels were unchanged. As Lis1 and Nudel also interact with and regulate dynein function, we quantified their levels in the optic nerve at P60 and found significant increases (Fig. 5, A and B). Similar results were found for the spinal cord (Fig. 5, C and D), whereas no difference between wild type and null was detected in the cerebral cortex (Fig. 5, E and F). mRNA levels for cytoplasmic dynein, as determined by RT-PCR, were not elevated in the retinae of *Plp* null mice (Fig. 5 G) at P60.

To show that the elevated levels of the retrograde motor proteins are related to the absence of PLP/DM20, we rescued the null phenotype by complementation with a wild-type *Plp* genomic transgene (Readhead et al., 1994; Griffiths et al., 1998). Levels of dynein and dynactin in the *Plp* null and wild-type mice expressing the transgene were the same as wild-type mice, whereas in the absence of the transgene the *Plp* null mice showed the expected elevations (unpublished data).

Although dynein and dynactin act to move cargoes in a retrograde direction, they themselves must first be transported anterogradely to the nerve terminal. Approximately 75% of anterograde movement is in the in the slow compo-

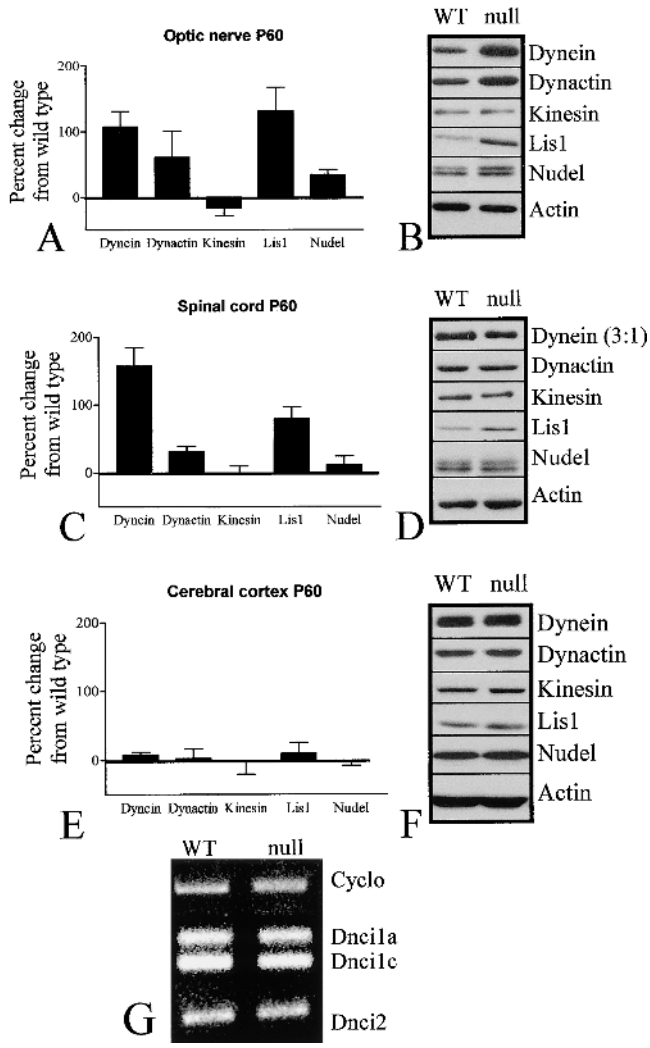

Figure 5. **Absence of PLP/DM20 is associated with elevated levels of retrograde motor proteins in affected regions.** (A–F) Steady-state levels of dynein intermediate chain, dynactin p50, kinesin heavy chain, Lis1, and Nudel in triton-extracted fractions of optic nerve (A and B), spinal cord (C and D), and cerebral cortex (E and F) of *Plp* null mice at P60. Bar charts (A, C, and E) show the percent change from wild-type littermates (M ± SEM; $n = 3–7$); panels (B, D, and F) show representative blots. The protein loading for dynein in the wild-type spinal cord is threefold greater than the null (3:1). In the optic nerve, all values except kinesin are significantly elevated in the *Plp* null mice. In the spinal cord dynein, dynactin and Lis1 are increased, whereas in the cerebral cortex there is no difference in any parameter (G). Representative RT-PCR of dynein intermediate chain genes 1 (Dnci1) and 2 (Dnci2) from retinae of P60 wild-type and *Plp* null mice. Two alternatively spliced Dnci1 transcripts (1a and 1c) are present. Cyclophilin (Cyclo) acts as an internal control. There is no difference in signals between the two genotypes.

nent b compartment, with the remainder in the fast component (Pfister, 1999; Susalka et al., 2000). To examine whether the elevated levels of dynein and dynactin might represent an effect on slow anterograde rather than retrograde movement, we measured levels of actin (Fig. 5 B) and spectrin, two main components of the slow component b compartments, in triton-soluble fractions of optic nerve. The values for both proteins in the optic nerve were not different from wild type at P20 and P60.

Late onset distal axonopathy occurs in *Plp* knockout and heterozygous mice and is not prevented by the *Wlds* allele

Significant tract degeneration is associated with long spinal pathways. At ~8 mo of age, early degeneration was seen in the fasciculus gracilis of the rostral cervical region, whereas no degeneration was observed in the rostral thoracic fasciculus gracilis until ~18 mo (Garbern et al., 2002). Therefore, we compared degeneration in the cervical fasciculus gracilis between wild-type mice, *Plp* null mice, and $Plp^{+/-}$ heterozygotes at 18 mo. Wild-type mice showed no evidence of degeneration (Fig. 6 A). The *Plp* null and heterozygous mice contained obvious degenerating fibers (Fig. 6, B and C), and although the frequency varied between different mice within a genotype, there was minimal overall qualitative difference between the amounts of degeneration in the two groups. The *Wlds* locus on chromosome 4 retards Wallerian degeneration after axonal damage, resulting in prolonged survival of the distal axon. By appropriate cross mating we generated *Plp* null mice expressing the *Wlds* allele, and at 4 and 18 mo of age determined if axonal changes were prevented or ameliorated. Axonal swellings in the optic nerve (unpublished data) and degeneration in the fasciculus gracilis (Fig. 6 D) were present and appeared identical in extent and distribution to those in the unmodified *Plp* null mice. We conclude that, at the ages examined, expression of the *Wlds* allele does not protect against the axonopathy induced by lack of PLP/DM20, in contrast to the peripheral neuropathy associated with P0 deficiency (Samsam et al., 2003).

Discussion

Impairment of axonal transport has emerged as a putative common factor in the pathogenesis of HSP (Crosby and Proukakis, 2002). Despite strong circumstantial evidence, conclusive proof has been absent, although recently a late impairment in transport has been verified in paraplegin-deficient mice (Ferreirinha et al., 2004). In this paper, we show that absence of the major myelin protein, PLP/DM20, from the oligodendrocyte, causes an early impairment of transport in the underlying axon, leading to multifocal accumulations of membranous organelles. Although this effect appears generalized, at least in smaller-diameter myelinated fibers, degeneration is concentrated at the distal regions of the longer axons. Traditionally, the main function of myelin has been viewed as the promotion of saltatory conduction. Increasingly, it is recognized that this is but one of many roles, and our analysis identifies a further function related to fast axonal transport and, furthermore, links this to a specific myelin molecule.

The oligodendrocyte provides local support for the axon

Two key observations indicate that the axonal changes are related to the absence of PLP/DM20 in the overlying myelin, and are not neuronally autonomous. Organelles accumulate only beneath the PLP/DM20-deficient myelin in $Plp^{+/-}$ heterozygotes and are absent in nonmyelinated axons. However, the presence of axonal swellings and organelle accumulations in the *shiverer* axons, only in association with

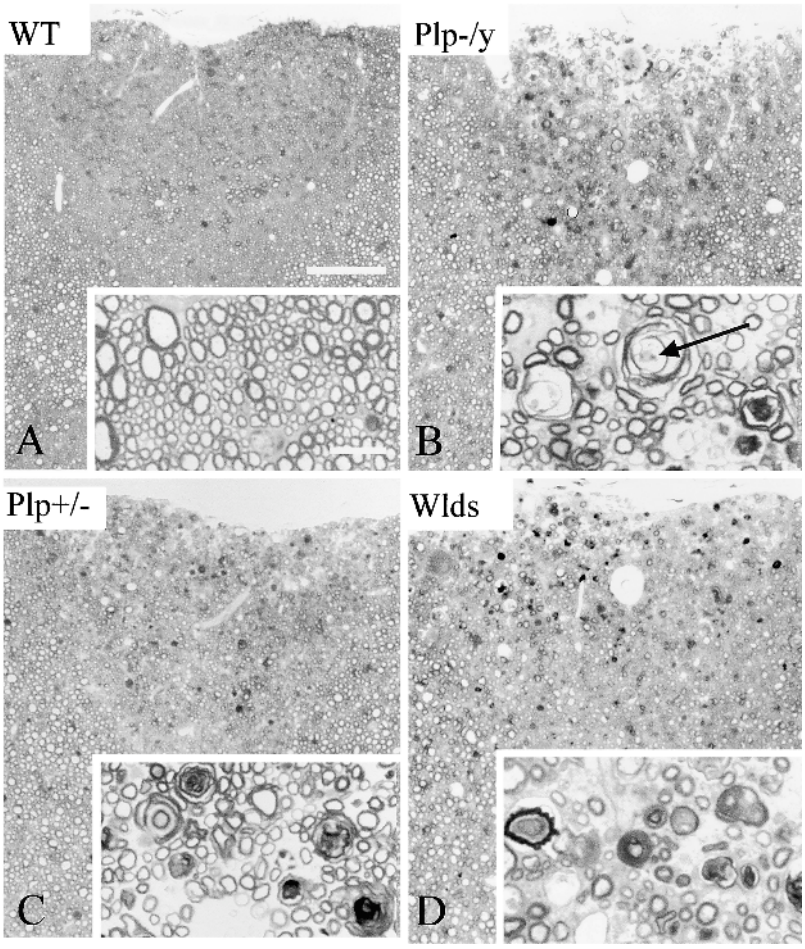

Figure 6. **Late-onset degeneration in the rostral cervical fasciculus gracilis of mice aged 18 mo.** (A) Wild-type (WT) mouse. (B) *Plp* null (Plp−/y) mouse showing axonal degeneration. (C) *Plp* heterozygous ($Plp^{+/-}$) mouse showing a pattern of degeneration very similar to that occurring in the null mouse. (D) *Plp* null mouse carrying the *Wlds* mutation (Wlds) that retards Wallerian degeneration after axonal transection. The pattern of axonal degeneration is very similar to that in the unmodified *Plp* null mouse, indicating the *Wlds* mutation provides no obvious protection. Bar, 50 μm. Insets: the fasciculus gracilis at higher power with the normal appearance in the wild-type mouse, and changes typical of axonal degeneration (arrow) in the other three genotypes. Bar, 10 μm.

the transplanted mutant oligodendrocytes, provides conclusive evidence that the PLP/DM20 deficiency is sufficient to cause the transport changes in the underlying axon.

With the major biosynthetic pathways localized in the neuronal soma, the axon is largely dependent on the cell body for maintenance. However, the ability of oligodendrocytes to influence the differentiation and maintenance of the axolemma is well recognized (Kordeli et al., 1990; Davis et al., 1996; Einheber et al., 1997; Menegoz et al., 1997; Rasband et al., 1999), and their effect on the major cytoskeletal elements has been linked to myelin status, being altered in hypomyelinating mutants (Brady et al., 1999). The localization of mitochondria within the axon has also been linked to the presence of overlying myelin (Bristow et al., 2002). Our data indicate novel, oligodendrocyte-dependent modulation of fast axonal transport systems, operating locally at the level of each myelinated internode. Furthermore, there is a strong indication that this process is not dependent on the volume of internodal myelin, per se, but on specific myelin molecules. This view is strengthened by our recent observation that absence of CNP, another myelin protein, results in a virtually identical axonopathy in the presence of normal myelin (Lappe-Siefke et al., 2003). The results suggest that oligodendrocytes communicate in some way with the underlying axon and support axonal function. A locally acting mechanism is compatible with the localization of spheroids to the PLP/DM20-deficient myelin in the $Plp^{+/-}$ heterozygotes and with the fact that few neuronal cell bodies degenerate in the *Plp* knockout mouse, the latter being a feature common to HSPs. In our mice, axon densities in the optic nerve and the size of the RGCs were identical between null and wild-type mice at 2 mo (an age at which retrograde transport was significantly impaired), and DiI labeling of RGCs of old mice via the nerve (unpublished data) indicated no apparent cell loss.

PLP/DM20 is necessary for fast transport in myelinated axons

The absence of PLP/DM20 from the overlying oligodendrocyte perturbs anterograde and retrograde axonal transport, although the organelle accumulation distal to nodes probably results from a defect in the latter. With regard to retrograde transport, the experiments using CTB-labeling periods of 6, 12, and 72 h suggest that initially, a proportion of axons is capable of transporting a reduced amount of substrate at a rate similar to the wild type; in other fibers transport is delayed or ceases completely. The most probable explanation is that retrograde transport is transiently delayed at affected nodal regions, which occur along the whole length of the visual pathway from the optic nerve to the colliculus. Eventually, transport arrests or is severely retarded in an individual fiber, and the number of blocked axons increases with age. In support of this, intensely fluorescent accumulations of CTB, with an appearance suggesting endosomal lo-

calization, were seen in optic nerve sections of *Plp* null mice, but rarely in wild-type mice. Interestingly, defects in endosomal function have been linked with other types of HSP or motorneuron disease (X.P. Zhao et al., 2001; Patel et al., 2002; Verhoeven et al., 2003; Yamanaka et al., 2003), suggesting that retrograde transport and membrane recycling processes are critical for neuronal survival. Although anterograde transport is impaired, we could detect no morphological correlate, such as accumulation of vesicular or tubular bodies at the proximal side of nodes. It may be that the spheroids act as a barrier to anterograde movement.

Absence of PLP/DM20 is associated with changes in levels of motor proteins

Kinesin and dynein are multi-subunit ATPases responsible for transport of membranous organelles and proteins along microtubules in the anterograde and retrograde directions, respectively. Dynein is associated with various adaptor and regulatory proteins including dynactin, Lis1, and Nudel. The optic nerve and spinal cord represent regions of the central nervous system that contain numerous axonal swellings; conversely, few swellings are present in the cerebral cortex. We find that steady-state levels of proteins in the dynein complex are elevated in triton-soluble extracts of the optic nerve and spinal cord of *Plp* null mice, whereas the cerebral cortex is not different from wild type. Kinesin levels are also unchanged at all locations. Therefore, the changes in retrograde motor proteins parallel the severity of the axonopathy. As there is no evidence of increased transcriptional activity in RGCs, the raised levels probably reflect the gradual accumulation of retrogradely moving organelles with their attached motor proteins. During the evolution of the axonopathy, one might envisage a retrogradely moving organelle reaching a particular nodal complex where it either "derails" from the microtubule or its further progress is blocked. We cannot exclude that some of the membranous bodies at the juxtaparanode are not transported from the axon terminal, but arise locally by invagination of the axolemma (Novotny, 1984). Such invaginations, which entrap oligodendrocyte membrane and cytoplasm, could also provide a potential glia-to-axon signaling pathway.

The significance of the elevated motor protein levels still has to be determined. However, mutations that disrupt either the dynein complex or kinesin result in failure of axonal transport, blockage of membranous cargoes, and axonal degeneration in both *Drosophila* and mammals (Hurd and Saxton, 1996; Martin et al., 1999; C. Zhao et al., 2001; LaMonte et al., 2002; Hafezparast et al., 2003).

Axonal degeneration is dependent on length of fiber and duration of disease

Only a small minority of optic axons in *Plp* null mice and humans ultimately degenerate despite the marked impairment in retrograde transport. In contrast, the distal regions of fibers in the cervical fasciculus gracilis and corticospinal tracts degenerate progressively (Garbern et al., 2002), suggesting that the length of the axon is critical in determining whether or not it will undergo degeneration. Over time, the extent of the degeneration tends to move proximally, toward the cell body, in a manner typical of a distal (dying back) axonopathy (Spencer and Schaumburg, 1976). Similar degeneration occurs in the fasciculus gracilis of $Plp^{+/-}$ heterozygotes in which ~66% of internodes are myelinated by PLP+ myelin (Yool et al., 2001). This indicates that, provided the axon is of sufficient overall length, only a minority of its distance needs to be associated with PLP/DM20-deficient myelin for distal degeneration to occur.

Is the late-onset distal degeneration related to transport defects? The kinesin and dynein mutants show that defects in anterograde or retrograde transport can precipitate axonal degeneration. Although we have not directly examined transport in the long spinal tracts, the morphological changes and transplant experiments suggest that transport is affected in a manner similar to the optic nerve. As axonal degeneration occurs at a time when both retrograde and anterograde transport are affected, it is not possible to state whether defects in one or both components is a probable precipitating factor. Alteration in axonal transport has been suggested as a common mechanism in the HSPs (Crosby and Proukakis, 2002) and in various other neurodegenerative disorders (Gunawardena et al., 2003; Hiruma et al., 2003; Szebenyi et al., 2003), although different pathways may lead to its compromise depending on the specific gene mutation. In most conditions the candidate gene is expressed predominantly in the neuron. Our findings also have implications for diseases considered as primary myelin disorders, such as multiple sclerosis. Axonal loss during the secondary progressive phase of multiple sclerosis has been attributed to loss of oligodendroglial/myelin support (Bjartmar et al., 2003), and our data establish that loss of oligodendroglial-specific molecules can indeed lead to functional impairment and loss of axons. The next step is to identify how these molecules influence axons and the downstream intra-axonal pathways.

Materials and methods

Mice

Plp null and wild-type male mice at P20, P60, P120, and various older ages up to 2 years were examined. These mice were on the C57BL/6 background, although the targeting event was performed on stem cells derived from 129SV mice. Genotyping was performed as described previously (Klugmann et al., 1997). Mice on the C57BL/6 background homozygous for the *Wlds* mutation were obtained commercially (Harlan UK Ltd.) and were crossed with the *Plp* knockout mice to obtain double mutants. For some experiments, female mice heterozygous for the *Plp* null allele were also used. *shiverer* mice on a C3H/101 background were used as transplant recipients.

Transgenic complementation of *Plp* null mice was achieved by cross mating female heterozygous $Plp^{+/-}$ mice with males from line 66 on a C57BL/6 background carrying a wild-type *Plp* genomic transgene (Readhead et al., 1994). Male offspring with and without the transgene were used.

Tissue collection and preparation

Mice for EM were perfused with glutaraldehyde/PFA and tissue from the second segment of the cervical spinal cord (C2) and mid-optic nerve was processed for resin embedding (Griffiths et al., 1981). Mice for immunocytochemistry were treated in various ways. For cryostat sections, mice were perfusion fixed with 4% PFA or Zamboni's fixative and tissue was cryoprotected in 20% sucrose. Tissue from other mice was dissected unfixed. All tissue was embedded in OCT compound (Sakura Fintek Europe) and snap frozen in isopentane cooled by liquid nitrogen. Cryosections were cut at 15 μm. For paraffin sections, mice were perfusion fixed in 4% PFA in phosphate buffer.

Collicular injections for retrograde transport

To study retrograde axonal transport, wild-type and *Plp* null male littermates at ages between 1 and 18 mo were injected with 1 μl of 1% fluorescein-conjugated CTB (Sigma-Aldrich) in sterile water with 2% DMSO. Injection was made into the right superior colliculus (Fig. 4 A) using stereotactic coordinates (bregma −3.6 mm caudally, −0.6 mm laterally, and −1.75 mm ventrally). After a defined interval, mice were perfused with 0.9% saline and the left retina was prepared as a whole mount (Hess, 1987) and fixed in 4% PFA in phosphate buffer. Between 12 and 16 digital images (IX70 microscope, Olympus; Color CoolView camera, Photonic Sciences) of each CTB-labeled retina were acquired. 3–4 positions between limbus and optic disc at 3–4 different locations around the retina were selected under phase optics, and the corresponding fluorescent image was stored. The total area occupied by fluorescent signal was determined within a defined area using Image-Pro Plus 4 software (Media Cybernetics); data are expressed as area of fluorescence per mm^2 of retina. The areas of RGC bodies were determined in P60 wild-type and *Plp* null retinae after immunostaining with the neuron-specific marker, β-tubulin III.

Intraocular injections for anterograde transport

To study anterograde axonal transport, 1 μl of [^{35}S]cysteine/methionine (Amersham Biosciences), specific activity 66 μCi/μl in sterile distilled water, was injected into the left eye of wild-type and *Plp* null male littermates at ages between P60 and 18 mo. The animals were maintained in the light for 12 h before the left retina and optic nerve and right optic tract, chiasm, and superior colliculus (Fig. 4 A) were dissected separately and homogenized in 10 mM Hepes with 1 mM EDTA and protease and phosphatase inhibitors (as for Western blotting). The homogenates were TCA precipitated, resuspended in 0.1 M Tris base to which a liquid scintillant (Ecoscint A; National Diagnostics) was added, and counted in a liquid scintillation counter (1900 Series; Packard). Collicular counts (disintegrations per minute) were expressed as a percentage of the total counts in all fractions.

Axonal morphometry and quantification of juxtaparanodal change

Axon diameter, density, and myelination status were assessed from electron micrographs (37,500×) of randomly selected fields of mid-optic nerve from 20-, 60-, and 120-d-old wild-type and *Plp* null mice (Yool et al., 2002b).

The frequency of axonal change at proximal and distal juxtaparanodal regions was assessed in longitudinal sections of optic nerve of three wild-type and five *Plp* null mice aged P40 (distal juxtaparanode refers to the juxtaparanode within a nodal–paranodal complex that is further from the neuronal cell body). Sections of optic nerve including the region of the retina and lamina cribrosa were examined in the electron microscope by an observer unaware of their genotype. Proximal and distal juxtaparanodal regions were identified in relation to the retina assuming all fibers were orientated in a retinal-to-chiasmal direction. The regions were qualitatively assigned as normal or abnormal in relation to the accumulation of membranous organelles.

Optic nerves from female $Plp^{+/-}$ heterozygotes were used to assess whether the accumulations of membranous organelles showed a preference to develop in association with internodes formed by PLP/DM20-deficient or wild-type myelin. Membranous accumulations were identified in longitudinal sections of optic nerve from groups of three mice aged P40 and 1 year using EM and were scored according to the nature of the intraperiod line of the associated myelin sheath (Boison and Stoffel, 1994; Rosenbluth et al., 1996; Klugmann et al., 1997).

Transplantation into the spinal cord of *shiverer* mice

Neurospheres (Zhang et al., 1998) from newborn (P1) wild-type or *Plp* null mice were dissociated into a single cell suspension and resuspended at a concentration of 50,000 cells/μl in L1 solution (Invitrogen). A thoracolumbar laminectomy was performed on *shiverer* pups aged between P14 and P21, and 2 μl of the suspension of wild-type or *Plp* null cells was injected into the dorsal columns of littermates using a glass microelectrode connected to a CellTram Oil manual piston pump (Eppendorf). The injection site was marked with sterile charcoal and the wound was sutured. After ∼4 mo, the mice were perfused with a PFA/glutaraldehyde mixture and longitudinal sections of the transplant site were prepared for resin embedding. 1-μm sections were immunostained for MBP and PLP and thin sections were prepared for EM. Seven *shiverer* mice transplanted with wild-type cells and four mice transplanted with *Plp* null cells established successful myelinated grafts and were used for analysis.

RT-PCR

RT-PCR was performed on retinae of four wild-type and *Plp* null mice at P60 for dynein intermediate chain gene 1 using published primers (Crackower et al., 1999) and gene 2 using forward primer 5′-ATTCAAGCAGGTGCTAAGCTGTCA-3′ and reverse primer 5′-TATTGCTGCGGTTATCCCAAAGCA-3′ (for full details see supplemental information, available at http://www.jcb.org/cgi/content/full/jcb.200312012/DC1).

Immunocytochemistry

Antibodies. PLP/DM20 was stained with a rabbit pAb to the common COOH terminus (271–276; donated by N.P. Groome, Oxford Brookes University, Oxford, UK), whereas PLP was stained with a pAb raised against a PLP-specific peptide sequence (117–129; donated by Dr. E. Trieflieff, Chimie Organique des Substances Naturelles, Strasbourg, France). In some experiments, PLP/DM20 was stained with a rat mAb against the COOH terminus (ImmunoDiagnostics, Inc.). NFs were stained with SMI-31 and SMI-32 (Sternberger Monoclonals, Inc.) recognizing phosphorylated and nonphosphorylated epitopes, respectively, of the NF-H and NF-M polypeptides. The RT97 antibody (Wood and Anderton, 1981), which recognizes a different phosphorylated epitope of the NF-H and NF-M proteins (Sánchez et al., 2000), was also used (donated by J.N. Wood, University College Medical School London, London, UK). NF-M, NF-L, and acetylated tubulin were stained with mAbs (Sigma-Aldrich). Caspr-1 was stained with a rabbit pAb (Einheber et al., 1997; donated by E. Peles, The Weizmann Institute of Science, Rehovot, Israel). Ankyrin G was stained with a mouse mAb (Zymed Laboratories). Filamentous actin was recognized by Bodipy-labeled phalloidin (Molecular Probes, Inc.). Neuronal spectrin was stained with a rabbit pAb (CHEMICON International). Potassium Kv1.1 channels and cytoplasmic dynein intermediate chain were stained with a pAb and mAb, respectively (CHEMICON International). Neurofascin was stained with an antibody provided by P.J. Brophy (University of Edinburgh, Edinburgh, UK; Tait et al., 2000). Dynactin p50 was recognized with a mouse mAb (BD Biosciences), kinesin heavy chain (H2) with a mouse mAb (CHEMICON International), β-actin, β-tubulin III, and APP were recognized with mouse mAbs (Sigma-Aldrich), Lis1 with rabbit and goat pAbs (donated by D. Smith [Harvard Medical School, Boston, MA] and from Santa Cruz Biotechnology, Inc.), Nudel with a rabbit pAb (donated by S. Hirotsune, Shirakawa Institute of Animal Genetics, Fukushima, Japan), and ubiquitin with a rabbit pAb (DakoCytomation).

Immunostaining. For most antibodies, cryosections were fixed in 4% PFA (for 20 min at 4°C), permeabilized in methanol (for 10 min at −20°C), and primary antibodies, diluted in PBS/1% normal goat serum, were applied overnight (at 4°C) either as single or double stains. Secondary FITC or Texas red–labeled conjugates diluted in the same buffer were applied for 30 min at RT. Staining for PLP/DM20 and the various NF antigens was also performed on tissue perfused with PFA or Zamboni's fixative. Sections were then permeabilized by 0.5% Triton X-100/PBS for 30 min at RT, and were blocked in 0.1% Triton X-100 and 0.2% pig skin gelatin in PBS. Primary and secondary antibodies were applied in the blocking buffer. When labeling with phalloidin, the cryosections were permeabilized in acetone. The various NF antibodies, APP, and ubiquitin were also used on paraffin sections in conjunction with the PAP technique. Resin sections of the transplanted spinal cords were immunostained for PLP and MBP using the PAP technique.

Western blotting

Mice were killed by CO_2 and brains (excluding the brain stem), spinal cords, and optic nerves from wild-type and *Plp* null male littermates at P20 and P60 were rapidly removed, snap frozen in liquid nitrogen, and stored at −80°C. Whole brain, cerebral cortices, and spinal cord were prepared using a modification of the method of Gotow et al. (1999), and optic nerves were divided into triton-soluble and -insoluble fractions (for details of fractionation procedures see supplemental information, available at http://www.jcb.org/cgi/content/full/jcb.200312012/DC1).

Protein concentrations were quantified using the BCA Protein Assay System (Pierce Chemical Co.). Proteins were loaded on 7.5, 10, or 14% acrylamide gels, subjected to SDS-PAGE, and transferred to Hybond™-P membrane (Amersham Biosciences) using a semi-dry blotting system. Blots were blocked in 5% skimmed milk in TBS (pH 7.4) and 0.1% Tween 20, incubated with various primary antibodies in blocking solution, washed, and then treated with HRP-labeled secondary antibodies (mouse HRP, Sigma-Aldrich; rabbit HRP, Scottish Antibody Production Unit, Law Hospital, Carluke, Scotland) and visualized using the ECL system (Pierce Chemical Co.). Autoradiographs were scanned and quantified using Scion Image for Windows (Scion Corporation).

Statistical analyses

The frequency of axonal changes in the proximal vs. distal juxtaparanode of knockout and wild-type optic nerves was compared using the Fisher's

exact test. The frequency distribution of RGC area was compared with the Chi-squared test. Levels of motor proteins in the central nervous system of paired wild-type and null littermates were compared using a paired *t* test. Other parameters between wild-type and knockout mice were compared with a two-tailed Mann-Whitney test (significance was defined as <0.05) (GraphPad Software).

Online supplemental material

Methods for RT-PCR and fractionation of tissue for Western blotting are listed. Fig. S1 and Fig. S2 show EM of optic nerve and oligodendrocytes transplanted to spinal cord, respectively. Online supplemental material available at http://www.jcb.org/cgi/content/full/jcb.200312012/DC1.

We are grateful to N.P. Groome and P.J. Brophy and to Drs. E. Trieflieff, J.N. Wood, D. Smith, S. Hirotsune, and E. Peles for antibodies; and to Dr. R.J.M. Franklin for advice.

This work was supported by Action Research (I.R. Griffiths), National MS Society (J. Garbern), and Deutsche Forschungsgemeinschaft SFB317 (K.A. Nave). J. Edgar was the recipient of a Bursary Award from the British Neuropathological Society.

Submitted: 1 December 2003
Accepted: 10 May 2004

References

Bjartmar, C., J.R. Wujek, and B.D. Trapp. 2003. Axonal loss in the pathology of MS: consequences for understanding the progressive phase of the disease. *J. Neurol. Sci.* 206:165–171.

Boison, D., and W. Stoffel. 1994. Disruption of the compacted myelin sheath of axons of the central nervous system in proteolipid protein-deficient mice. *Proc. Natl. Acad. Sci. USA.* 91:11709–11713.

Boison, D., H. Büssow, D. D'Urso, H.-W. Müller, and W. Stoffel. 1995. Adhesive properties of proteolipid protein are responsible for the compaction of CNS myelin sheaths. *J. Neurosci.* 15:5502–5513.

Brady, S.T., A.S. Witt, L.L. Kirkpatrick, S.M. De Waegh, C. Readhead, P.H. Tu, and V.M.Y. Lee. 1999. Formation of compact myelin is required for maturation of the axonal cytoskeleton. *J. Neurosci.* 19:7278–7288.

Bristow, E.A., P.G. Griffiths, R.M. Andrews, M.A. Johnson, and D.M. Turnbull. 2002. The distribution of mitochondrial activity in relation to optic nerve structure. *Arch. Ophthalmol.* 120:791–796.

Crackower, M.A., D.S. Sinasac, J. Xia, J. Motoyama, M. Prochazka, J.M. Rommens, S.W. Scherer, and L.C. Tsui. 1999. Cloning and characterization of two cytoplasmic dynein intermediate chain genes in mouse and human. *Genomics.* 55:257–267.

Crosby, A.H., and C. Proukakis. 2002. Is the transportation highway the right road for hereditary spastic paraplegia? *Am. J. Hum. Genet.* 71:1009–1016.

Davis, J.Q., S. Lambert, and V. Bennett. 1996. Molecular composition of the node of Ranvier: Identification of ankyrin-binding cell adhesion molecules neurofascin (Mucin+ third FNIII domain−) and NrCAM at nodal axon segments. *J. Cell Biol.* 135:1355–1367.

Einheber, S., G. Zanazzi, W. Ching, S. Scherer, T.A. Milner, E. Peles, and J.L. Salzer. 1997. The axonal membrane protein Caspr, a homologue of neurexin IV, is a component of the septate-like paranodal junctions that assemble during myelination. *J. Cell Biol.* 139:1495–1506.

Ferreirinha, F., A. Quattrini, M. Pirozzi, V. Valsecchi, G. Dina, V. Broccoli, A. Auricchio, F. Piemonte, G. Tozzi, L. Gaeta, et al. 2004. Axonal degeneration in paraplegin-deficient mice is associated with abnormal mitochondria and impairment of axonal transport. *J. Clin. Invest.* 113:231–242.

Fink, J.K. 2002. Hereditary spastic paraplegia: The pace quickens. *Ann. Neurol.* 51: 669–672.

Garbern, J., D.A. Yool, G.J. Moore, I. Wilds, M. Faulk, M. Klugmann, K.-A. Nave, E.A. Sistermans, M.S. van der Knaap, T.D. Bird, et al. 2002. Patients lacking the major CNS myelin protein, proteolipid protein 1, develop length-dependent axonal degeneration in the absence of demyelination and inflammation. *Brain.* 125:551–561.

Gotow, T., J.F. Leterrier, Y. Ohsawa, T. Watanabe, K. Isahara, R. Shibata, K. Ikenaka, and Y. Uchiyama. 1999. Abnormal expression of neurofilament proteins in dysmyelinating axons located in the central nervous system of jimpy mutant mice. *Eur. J. Neurosci.* 11:3893–3903.

Griffiths, I.R., I.D. Duncan, and M. McCulloch. 1981. Shaking pup: a disorder of central myelination in the spaniel dog. II. Ultrastructural observations on the white matter of cervical spinal cord. *J. Neurocytol.* 10:847–858.

Griffiths, I.R., M. Klugmann, T.J. Anderson, D. Yool, C.E. Thomson, M.H. Schwab, A. Schneider, F. Zimmermann, M.C. McCulloch, N.L. Nadon, and K.-A. Nave. 1998. Axonal swellings and degeneration in mice lacking the major proteolipid of myelin. *Science.* 280:1610–1613.

Gunawardena, S., L.S. Her, R.G. Brusch, R.A. Laymon, I.R. Niesman, B. Gordesky-Gold, L. Sintasath, N.M. Bonini, and L.S. Goldstein. 2003. Disruption of axonal transport by loss of huntingtin or expression of pathogenic polyQ proteins in *Drosophila*. *Neuron.* 40:25–40.

Hafezparast, M., R. Klocke, C. Ruhrberg, A. Marquardt, A. Ahmad-Annuar, S. Bowen, G. Lalli, A.S. Witherden, H. Hummerich, S. Nicholson, et al. 2003. Mutations in dynein link motor neuron degeneration to defects in retrograde transport. *Science.* 300:808–812.

Hess, D.T. 1987. A retinal whole-mount method useful in detecting retrogradely-labeled ganglion cells. *Brain Res. Bull.* 18:581–584.

Hiruma, H., T. Katakura, S. Takahashi, T. Ichikawa, and T. Kawakami. 2003. Glutamate and amyloid β-protein rapidly inhibit fast axonal transport in cultured rat hippocampal neurons by different mechanisms. *J. Neurosci.* 23: 8967–8977.

Hurd, D.D., and W.M. Saxton. 1996. Kinesin mutations cause motor neuron disease phenotypes by disrupting fast axonal transport in *Drosophila*. *Genetics.* 144:1075–1085.

Kirkpatrick, L.L., A.S. Witt, H.R. Payne, H.D. Shine, and S.T. Brady. 2001. Changes in microtubule stability and density in myelin-deficient shiverer mouse CNS axons. *J. Neurosci.* 21:2288–2297.

Klugmann, M., M.H. Schwab, A. Pühlhofer, A. Schneider, F. Zimmermann, I.R. Griffiths, and K.-A. Nave. 1997. Assembly of CNS myelin in the absence of proteolipid protein. *Neuron.* 18:59–70.

Kordeli, E., J. Davis, B.D. Trapp, and V. Bennett. 1990. An isoform of ankyrin is localized at nodes of Ranvier in myelinated axons of central and peripheral nerves. *J. Cell Biol.* 110:1341–1352.

LaMonte, B.H., K.E. Wallace, B.A. Holloway, S.S. Shelly, J. Ascaño, M. Tokito, T. Van Winkle, D.S. Howland, and E.L.F. Holzbaur. 2002. Disruption of dynein/dynactin inhibits axonal transport in motor neurons causing late-onset progressive degeneration. *Neuron.* 34:715–727.

Lappe-Siefke, C., S. Goebbels, M. Gravel, E. Nicksch, J. Lee, P.E. Braun, I.R. Griffiths, and K.-A. Nave. 2003. Disruption of the *CNP* gene uncouples oligodendroglial functions in axonal support and myelination. *Nat. Genet.* 33: 366–374.

Martin, M., S.J. Iyadurai, A. Gassman, J.G. Gindhart, T.S. Hays, and W.M. Saxton. 1999. Cytoplasmic dynein, the dynactin complex and kinesin are interdependent and essential for fast axonal transport. *Mol. Biol. Cell.* 10:3717–3728.

Menegoz, M., P. Gaspar, M. Le Bert, T. Galvez, F. Burgaya, C. Palfrey, P. Ezan, F. Amos, and J.A. Girault. 1997. Paranodin, a glycoprotein of neuronal paranodal membranes. *Neuron.* 19:319–331.

Novotny, G.E. 1984. Formation of cytoplasm-containing vesicles from double-walled coated invaginations containing oligodendrocytic cytoplasm at the axon-myelin sheath interface in adult mammalian central nervous system. *Acta Anat. (Basel).* 119:106–112.

Patel, H., H. Cross, C. Proukakis, R. Hershberger, P. Bork, F.D. Ciccarelli, M.A. Patton, V.A. McKusick, and A.H. Crosby. 2002. *SPG20* is mutated in Troyer syndrome, an hereditary spastic paraplegia. *Nat. Genet.* 31:347–348.

Peles, E., and J.L. Salzer. 2000. Molecular domains of myelinated axons. *Curr. Opin. Neurobiol.* 10:558–565.

Pfister, K.K. 1999. Cytoplasmic dynein and microtubule transport in the axon: The action connection. *Mol. Neurobiol.* 20:81–91.

Rasband, M.N., J.S. Trimmer, E. Peles, S.R. Levinson, and P. Shrager. 1999. K^+ channel distribution and clustering in developing and hypomyelinated axons of the optic nerve. *J. Neurocytol.* 28:319–331.

Readhead, C., A. Schneider, I.R. Griffiths, and K.-A. Nave. 1994. Premature arrest of myelin formation in transgenic mice with increased proteolipid protein gene dosage. *Neuron.* 12:583–595.

Reid, E. 2003. Science in motion: common molecular pathological themes emerge in the hereditary spastic paraplegias. *J. Med. Genet.* 40:81–86.

Reid, E., M. Kloos, A. Ashley-Koch, L. Hughes, S. Bevan, I.K. Svenson, F.L. Graham, P.C. Gaskell, A. Dearlove, M.A. Pericak-Vance, et al. 2002. A kinesin heavy chain (*KIF5A*) mutation in hereditary spastic paraplegia (SPG10). *Am. J. Hum. Genet.* 71:1189–1194.

Rosenbluth, J., W. Stoffel, and R. Schiff. 1996. Myelin structure in proteolipid protein (PLP)-null mouse spinal cord. *J. Comp. Neurol.* 371:336–344.

Samsam, M., W. Mi, C. Wessig, J. Zielasek, K.V. Toyka, M.P. Coleman, and R. Martini. 2003. The wlds mutation delays robust loss of motor and sensory

axons in a genetic model for myelin-related axonopathy. *J. Neurosci.* 23: 2833–2839.

Sánchez, I., L. Hassinger, R.K. Sihag, D.W. Cleveland, P. Mohan, and R.A. Nixon. 2000. Local control of neurofilament accumulation during radial growth of myelinating axons in vivo: Selective role of site-specific phosphorylation. *J. Cell Biol.* 151:1013–1024.

Spencer, P.S., and H.H. Schaumburg. 1976. Central-peripheral distal axonopathy—the pathology of dying-back polyneuropathies. *Prog. Neuropath.* 3: 253–295.

Susalka, S.J., W.O. Hancock, and K.K. Pfister. 2000. Distinct cytoplasmic dynein complexes are transported by different mechanisms in axons. *Biochim. Biophys. Acta.* 1496:76–88.

Szebenyi, G., G.A. Morfini, A. Babcock, M. Gould, K. Selkoe, D.L. Stenoien, M. Young, P.W. Faber, M.E. MacDonald, M.J. McPhaul, and S.T. Brady. 2003. Neuropathogenic forms of huntingtin and androgen receptor inhibit fast axonal transport. *Neuron.* 40:41–52.

Tait, S., F. Gunn-Moore, J.M. Collinson, J. Huang, C. Lubetzki, L. Pedraza, D.L. Sherman, D.R. Colman, and P.J. Brophy. 2000. An oligodendrocyte cell adhesion molecule at the site of assembly of the paranodal axo-glial junction. *J. Cell Biol.* 150:657–666.

Tsukita, S., and H. Ishikawa. 1980. The movement of membranous organelles in axons. Electron microscopic identification of anterogradely and retrogradely transported organelles. *J. Cell Biol.* 84:513–530.

Verhoeven, K., D. De Jonghe, K. Coen, N. Verpoorten, M. Auer-Grumbach, J.M. Kwon, D. FitzPatrick, E. Schmedding, E. De Vriendt, A. Jacobs, et al. 2003. Mutations in the small GTP-ase late endosomal protein RAB7 cause Charcot-Marie-Tooth type 2B neuropathy. *Am. J. Hum. Genet.* 72:722–727.

Wood, J.N., and B.H. Anderton. 1981. Monoclonal antibodies to mammalian neurofilaments. *Biosci. Rep.* 1:263–268.

Yamanaka, K., C.V. Velde, E. Eymard-Pierre, E. Bertini, O. Boespflug-Tanguy, and D.W. Cleveland. 2003. Unstable mutants in the peripheral endosomal membrane component ALS2 cause early-onset motor neuron disease. *Proc. Natl. Acad. Sci. USA.* 100:16041–16046.

Yool, D.A., M. Klugmann, M. McLaughlin, D.A. Vouyiouklis, L. Dimou, J.A. Barrie, M.C. McCulloch, K.-A. Nave, and I.R. Griffiths. 2001. Myelin proteolipid proteins promote the interaction of oligodendrocytes and axons. *J. Neurosci. Res.* 63:151–164.

Yool, D., M. Klugmann, J.A. Barrie, M.C. McCulloch, K.-A. Nave, and I.R. Griffiths. 2002a. Observations on the structure of myelin lacking the major proteolipid protein. *Neuropathol. Appl. Neurobiol.* 28:75–78.

Yool, D., P. Montague, M. McLaughlin, M.C. McCulloch, J.M. Edgar, K.A. Nave, R.W. Davies, I.R. Griffiths, and A.S. McCallion. 2002b. Phenotypic analysis of mice deficient in the major myelin protein MOBP, and evidence for a novel *Mobp* isoform. *Glia.* 39:256–267.

Zhang, S.C., C. Lundberg, D. Lipsitz, L.T. O'Connor, and I.D. Duncan. 1998. Generation of oligodendroglial progenitors from neural stem cells. *J. Neurocytol.* 27:475–489.

Zhao, C., J. Takita, Y. Tanaka, M. Setou, T. Nakagawa, S. Takeda, H.W. Yang, S. Terada, T. Nakata, Y. Takei, et al. 2001. Charcot-Marie-Tooth disease type 2A caused by mutation in a microtubule motor KIF1Bβ. *Cell.* 105:587–597.

Zhao, X.P., D. Alvarado, S. Rainier, R. Lemons, P. Hedera, C.H. Weber, T. Tukel, M. Apak, T. Heiman-Patterson, L. Ming, et al. 2001. Mutations in a newly identified GTPase gene cause autosomal dominant hereditary spastic paraplegia. *Nat. Genet.* 29:326–331.